

## Combined Machining of Ti-6Al-4V Alloy Using Electrochemical Milling and Electrochemical Grinding

Gangqiang Liu, Hansong Li\*, Shen Niu, Xiaokang Yue and Ningsong Qu

National Key Laboratory of Science and Technology on Helicopter Transmission, Nanjing, China, 210016

\*E-mail: [hsli@nuaa.edu.cn](mailto:hsli@nuaa.edu.cn)

Received: 28 March 2019 / Accepted: 16 July 2019 / Published: 30 August 2019

---

Ti-6Al-4V is a typical difficult-to-cut material with which it is difficult to achieve a high processing efficiency and good surface quality simultaneously using a single processing method. In this paper, a combined method that consists of electrochemical milling and grinding is proposed to solve this problem. Two types of electrodes were used in the different machining stages. First, the polarization curves for Ti-6Al-4V in 10% NaNO<sub>3</sub> solution were obtained. Then, the maximum feed and material removal rates were studied using various electrochemical milling parameters. The resulting machined groove cross-sectional profiles were compared. Finally, the effects of electrochemical grinding on the machining results were investigated. The machined workpiece surfaces were examined using scanning electron microscopy and their roughnesses were measured using a roughometer.

---

**Keywords:** Ti-6Al-4V alloy; Electrochemical milling; Electrochemical grinding; material removal rate; surface roughness

### 1. INTRODUCTION

Ti-6Al-4V is widely used in the aviation industry due to its low density, high specific strength, thermal resistance, and corrosion resistance. It accounts for approximately 50% of titanium alloy production [1-4]. Due to its low elastic modulus, low deformation coefficient, severe chilling phenomenon, and high cutting temperature, tool wear occurs quickly during traditional cutting processes [5]. Therefore, machining Ti-6Al-4V via traditional processing methods is difficult.

Electrochemical machining is based on the principle of electrochemical anode dissolution, which produces no tool wear, no residual stress on the machined surface, no burr, etc. Thus, the processing efficiency associated with electrochemical machining is high and it is suitable for processing of difficult-to-cut materials [6]. Electrochemical milling uses an electrode with a simple shape to form a machined

surface along its path of movement. This makes it a highly flexible processing method [7]. Hinduja and Pattavanitch [8] produced a complex stainless steel surface structure using electrodes with different cross-sections. Liu et al. [9] studied the machining of TB6 titanium alloy using a metal nozzle with a 2 mm inner diameter and found that the cathode feed rate was 1.5 mm/min. Wang et al. [10] used a tubular cathode to process Inconel 718 alloy and found that the cathode feed rate was 4 mm/min. Vanderauwera et al. [11] used a tubular cathode and an external nozzle to perform layer-by-layer processing on stainless steel, achieving a processing depth of 0.8 mm.

In the above-mentioned electrochemical milling technologies, researchers have focused primarily on forming regularity at the bottom surface. They have relied on the end of the cathode to provide the electric field and the depth of material removal during each pass is quite small. As a result, it is necessary to adopt multiple layer-by-layer processing methods so as to achieve a desired removal depth. In order to improve the processing depth of a single pass, Liu et al. [12] designed slanted spray holes on the hemispherical cathode surface, producing a round raceway in a GCr15 steel workpiece with a machining depth of 2.5 mm and a feed rate of 0.3 mm/min. Niu et al. [13] used a spray slit on the sidewall of a tubular cathode to process a thin-walled structure on Inconel 718 with a machining depth of 3 mm and a feed rate of 2.1 mm/min.

The machined surface is inevitably affected by stray current, resulting in poor surface quality and precision control. This makes meeting finishing requirements difficult [14,15]. Electrochemical grinding is a compound process that achieves material removal via a combination of electrolysis and grinding [16]. Unlike in electrolytic machining, the oxide film formed on the workpiece surface can be quickly scraped away by abrasive particles on a conductive grinding wheel. This exposes a new metal surface to electrolysis. Hascalik and Caydas [17] used electrochemical grinding to improve the surface roughness of Ti-6Al-4V after electrical discharge machining. Curtis et al. [18] studied machining of nickel-base superalloys via electrochemical grinding and produced leaf discs with surface roughnesses of 0.65  $\mu\text{m}$ . Clearly, electrochemical grinding is an effective method of achieving good surface quality.

In order to achieve efficient Ti-6Al-4V alloy processing with better surface quality, we propose an innovative method that combines electrochemical milling and electrochemical grinding using the same tool substrate in this paper. The principle of combined processing is introduced. In addition, the maximum feed and material removal rates associated with various machining parameters are studied. The cross-sectional profiles of machined grooves are compared, machined surfaces are examined, and the surface roughness is measured.

## 2. THE COMBINED MACHINING METHOD

### 2.1 Principle of combined machining

Fig. 1 shows a schematic of combined machining. The combined processing sequence consisted of two stages: electrochemical milling and electrochemical grinding. Stage 1 took advantage of the high material removal rate associated with electrochemical milling and stage 2 utilized the good surface quality provided by electrochemical grinding.

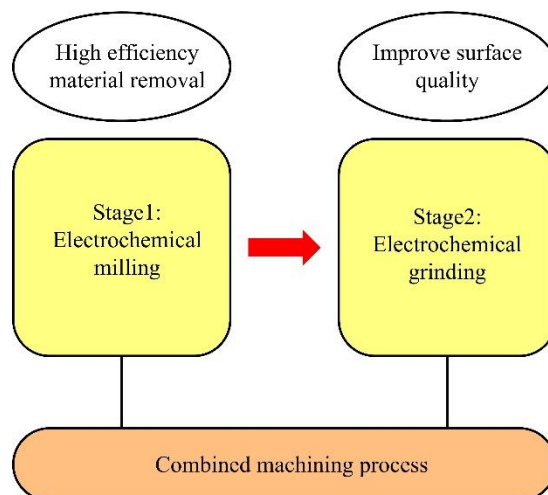


**Figure 1.** Schematic diagram of the combined processing sequence.

The main purpose of the pre-machining step was to achieve high-efficiency machining of Ti-6Al-4V via electrochemical milling. Electrochemical milling is based on the principle of electrochemical anode dissolution and benefits from the flexibility of numerical control technology.

The schematic diagram in Fig. 2 shows pre-machining via inner-jet electrochemical milling. The electrode moved along a specified trajectory while rotating quickly. The electrolyte was sprayed from the hole at the bottom of the electrode to the processing area, connecting the electrode and the workpiece to form a conducting circuit. The electrolyte removed reaction byproducts and Joule heat from the machining area simultaneously.

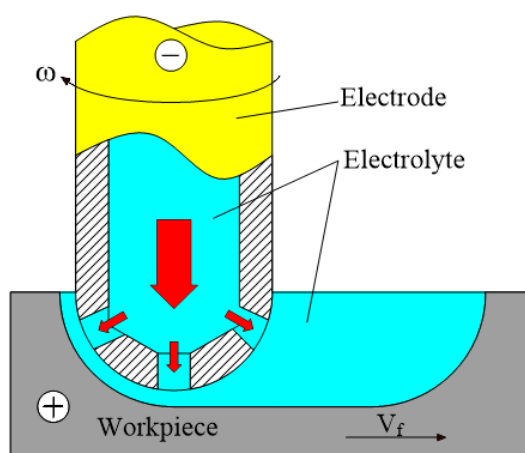


**Figure 2.** Schematic diagram of inner-jet electrochemical milling.

Although the machining efficiency was high during the pre-machining stage, the resulting surfaces were rough. Thus, electrochemical grinding was adopted to improve the surface quality and meet finishing or semi-finishing requirements.

Fig. 3 shows a schematic diagram of inner-jet electrochemical grinding, which uses a combination of electrochemical action and mechanical grinding. The electrode used for pre-machining is also the abrasive tool substrate used in post-machining. To prepare the abrasive tool, diamond particles were fastened to the tool surface via electrodeposition. The gap between the bottom of the abrasive tool

and the workpiece decreased since the abrasive tool was fed downwards until the surfaces were in contact. The diamond particles removed the non-reactive passivation layer, exposing fresh metal to the electrolytic reaction.

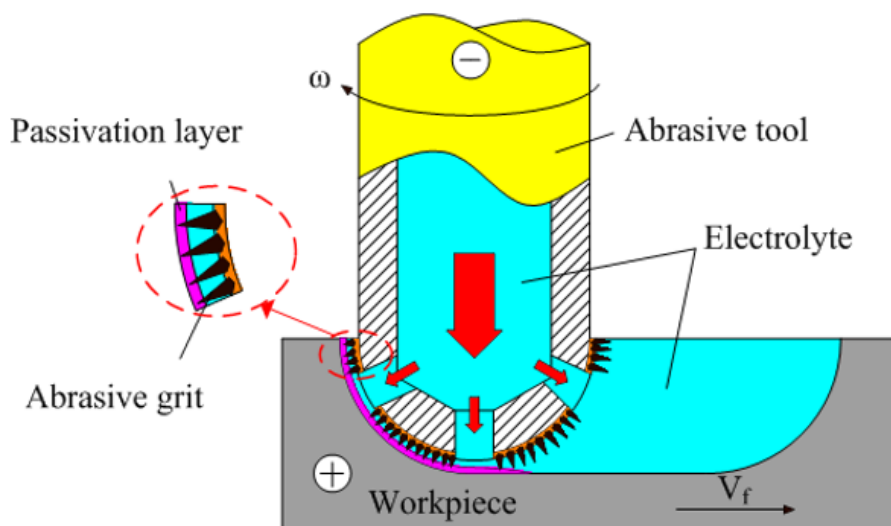


**Figure 3.** Schematic diagram of inner-jet electrochemical grinding.

### 3. EXPERIMENTAL PROCEDURES

Anodic polarization curves were measured using a three-electrode setup and an electrochemical workstation (Zennium E, Zahner, Germany). A platinum electrode and a calomel electrode were used as the counter and reference electrodes, respectively. The working electrode was a Ti-6Al-4V cube with dimensions of 10 mm × 10 mm × 10 mm. One surface of the cube was pretreated with abrasive paper and then cleaned with distilled water. The remaining surfaces were covered with resin. During the experiments, the electrolyte temperature was set to 30 °C and the tests were performed potentiodynamically over the -2 V to 16 V range. The sweep rate was 10 mV/s.

As shown in Fig. 4, the main components of the machining system were the machine body, motion control system, data acquisition system, electrolyte system, and power supply. In particular, a tool cathode with through holes and rotary joints was used to perform internal flushing. The motion control system consisted of a computer, a servo motor, a servo drive, and a motion control card, and was used to control the workpiece and the spindle feed rates. Hall current sensors and data acquisition cards were used to monitor and record the machining currents. In addition, pressure sensors were used to monitor the electrolyte pressure during processing.

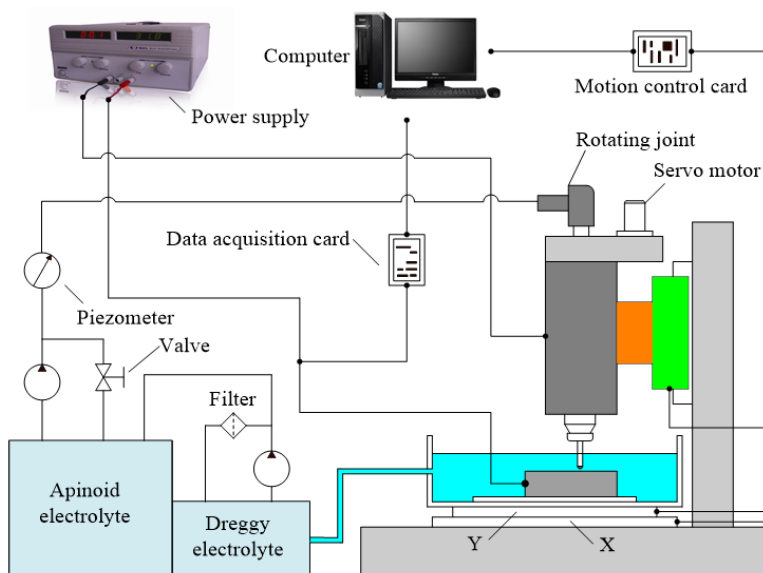


**Figure 4.** Schematic diagram of the experimental system.

The material removal rate (MRR) is one of the most important machining efficiency criteria and is defined as follows:

$$MRR = \frac{\Delta V}{t} \tag{1}$$

where  $\Delta V$  is the volume removed during processing and  $t$  is the total processing time.

**Table 1.** Ti-6Al-4V composition (wt %)

Ti	Al	V	Fe	O	C	N	H
89.36	6	4	0.3	0.2	0.08	0.05	0.01

Table 1 shows the chemical composition of the Ti-6Al-4V alloy used in this study. Table 2 shows the machining conditions used in the tests. We used a 10 wt% NaNO<sub>3</sub> solution as the electrolyte. The electrolyte temperature was set to 30 °C and the grinding wheel rotation speed was 1000 rpm.

**Table 2.** Machining conditions.

Parameter	Value
Workpiece size (mm)	110×90×10
Electrolyte type	NaNO <sub>3</sub> (10 wt%)
Electrolyte temperature (°C)	30
Spindle rotation rate (rpm)	1000
Electrolyte pressure (MPa)	0.2/0.6
Tool type	A/B

Fig. 5 shows photographs of the two columnar electrodes: tool A and tool B. Each tool electrode substrate was made from carbon steel. Tool A was a hollow metal bar with a hemispherical end. The

inside and outside diameters of the bar were 4 mm and 6 mm, respectively. In addition, seven small holes (1 mm diameter) were uniformly distributed on the hemispherical bottom of tool A to ensure that the electrolyte entered the processing area uniformly. Tool B was produced by electroplating a diamond abrasive layer on the hemispherical bottom surface of tool A. The diamond particle size and concentration were approximately 75–90  $\mu\text{m}$  and 8.8 carat  $\text{cm}^{-3}$ , respectively. The thickness and height of the electrodeposit were approximately 0.1 mm and 5 mm, respectively. A scanning electron microscope (S-3400N, Hitachi, Japan) was used to study the quality of the machined surface. A roughometer (Perthometer M1, Mahr, Germany) was used to measure the surface roughness. The cross-sectional profiles of all machined slots were measured using a coordinate measuring instrument (ZEISS CONTURA, Germany) and cross-sectional photographs of all machined slots were captured using a three-dimensional profilometer (DVM5000, Leica, Germany).



**Figure 5.** Photographs of the columnar electrodes: (a) tool A and (b) tool B.

## 4. RESULTS AND DISCUSSION

### 4.1 Selection of electrolysis parameters

Titanium is self-passivating and thus the passive film formed on the surface impedes dissolution of the base metal [19,20]. Therefore, it is important to choose appropriate electrolysis parameters in order to achieve a stable, efficient process. Fig. 6 shows Ti-6Al-4V polarization curves measured in a 10%  $\text{NaNO}_3$  solution. When the potential exceeds 11 V, the current density increases gradually, indicating that electrochemical dissolution is occurring on the anode surface. The current density increases rapidly when the potential exceeds 12 V. However, the current density increases little when the potential exceeds 13 V. Therefore, in order to optimize the pre-machining efficiency, the applied voltage should be no less than 13 V. Based on this, the applied voltage was varied from 15 V to 30 V in four equal steps.

The post-machining stage is not expected to remove large quantities of workpiece materials. Its main purpose is to improve the surface quality via electrochemical grinding. In electrochemical machining, a passive film that can impede unwanted workpiece dissolution is typically formed on the

surface at low current densities in  $\text{NaNO}_3$  solution [21-23]. Therefore, it is necessary to choose a low processing voltage for the post-machining stage. In this paper, the applied voltage is 1 V and the workpiece feed rate is  $30 \text{ mm}\cdot\text{min}^{-1}$ .

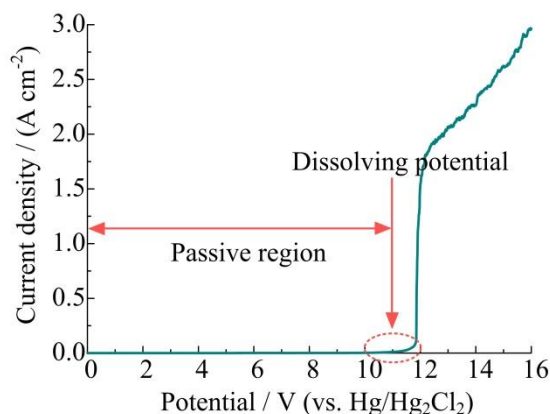


**Figure 6.** Polarization curve for Ti-6Al-4V in a 10%  $\text{NaNO}_3$  solution at  $30 \text{ }^\circ\text{C}$ .

#### 4.2 Pre-machining via electrochemical milling

In this pair of experiments, the maximum feed rate of tool A was determined under various machining parameters. We then used tool A to machine experimental grooves so that we could study machining results under various processing parameters. First, tool A was set to move 3 mm in the vertical direction at  $0.8 \text{ mm}/\text{min}$  before feeding horizontally at the previously measured maximum feed rate. The machined grooves were 20 mm-long. The machining conditions are shown in Table 3.

**Table 3.** Pre-machining parameters

Parameter	Value
Tool type	A
Applied voltage, V	15,20,25,30
Electrolyte pressure, MPa	0.6
Machining length, mm	20
Cutting depth, mm	3
Electrolyte temperature, $^\circ\text{C}$	30

Fig. 7 shows how the maximum feed rate and MRR vary with the applied voltage. The maximum feed rate increases from  $1.2 \text{ mm}\cdot\text{min}^{-1}$  to  $2.2 \text{ mm}\cdot\text{min}^{-1}$  as the applied voltage increases from 15 V to 30 V. The MRR increases from  $22.88 \text{ mm}^3\cdot\text{min}^{-1}$  to  $40.62 \text{ mm}^3\cdot\text{min}^{-1}$  over the same voltage range. One can conclude that increasing the applied voltage within the 15 V–30 V range serves to improve processing efficiency during pre-machining.

Mishra et al. [24] obtained ‘L’ shaped features on Ti-6Al-4V via layer-by-layer electrochemical milling at a feed rate of  $2.4 \text{ mm}/\text{min}$ , achieving a processing depth of 0.6 mm (single layer depth: 0.2 mm). In order to reflect the machining area per unit time, we constructed a product of the feed rate and

processing depth. It is clear that even the lowest value in this work is higher than in the work by K. Mishra. Obviously, the inner-jet electrochemical milling method presented in this paper is more suitable for the removal of large quantities of material than that which was presented previously.

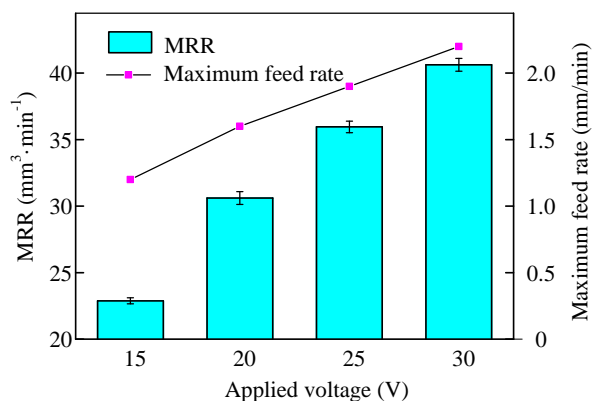


**Figure 7.** Maximum feed rate and MRR variation with the applied voltage.

Fig. 8 shows the time-current curve of the pre-machining process. The curves produced using different applied voltages are smooth throughout the machining process, which indicates that electrochemical machining is stable under the selected machining parameters. In addition, the current increases and the machining time decreases as the applied voltage increases. An applied voltage of 30 V provides a machining time of less than 800 s. Thus, 30 V is a suitable voltage for processing efficiency and stability.

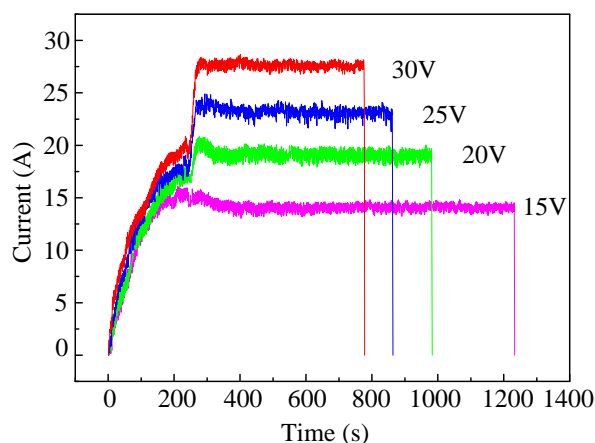


**Figure 8.** Comparison of machining currents produced under different applied voltages.

Fig. 9 and Fig.10 show cross-sectional photographs and profiles, respectively, of grooves machined using a variety of applied voltages. One can see that the cross-sectional profile varies with the voltage: higher voltages (within the 15 V–30 V range) produce deeper machined slots. When the voltage is increased from 15 V to 30 V, the maximum groove depth increases from 3.48 mm to 3.81 mm. However, actual average groove depths often exceed the preset electrode cut depth because of electrochemical dissolution [25,26]. The electrolyte may be sprayed onto the machined surface due to

rotation of tool A, which results in the generation of spray current. Therefore, material removal continues on the machined area even after the electrode has moved away. This deepens the machined grooves. This process is called stray removal [27]. According to Faraday’s law, the anode mass removed is directly proportional to number of electrons processed. As the applied voltage increases, additional workpiece material dissolution occurs due to the increased processing current. Hence, the maximum groove depth increases. The percentage by which the actual cutting profile exceeds that which was set increases from 16% to 27% when the voltage increases from 15 V to 30 V.

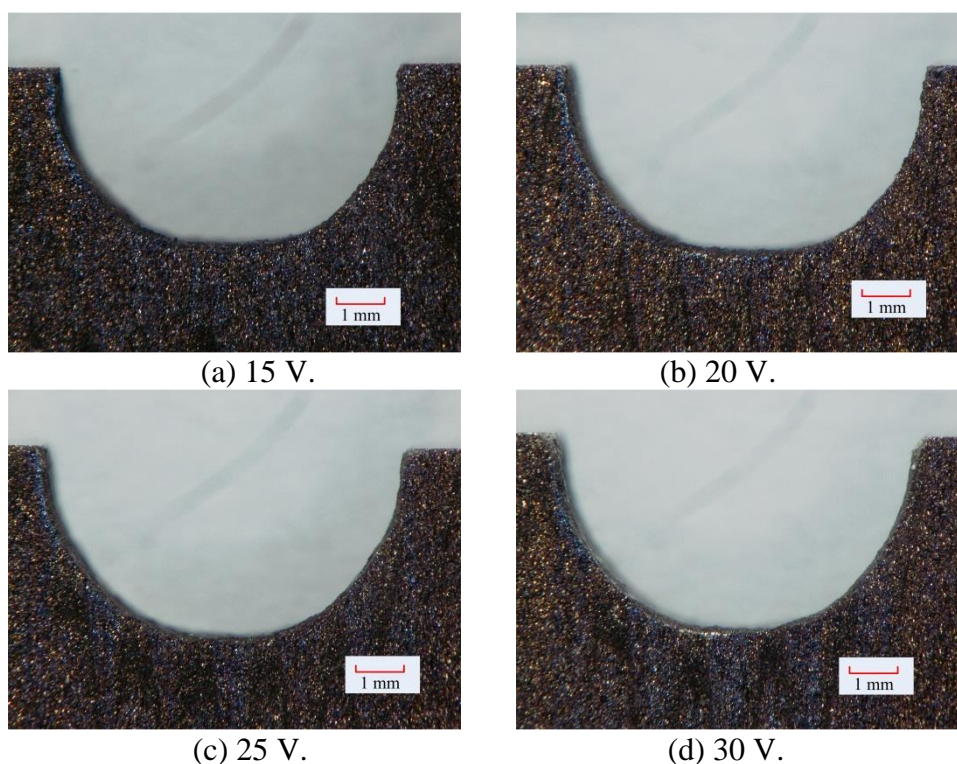


Figure 9. Cross-sectional photographs of machined grooves under different voltages.

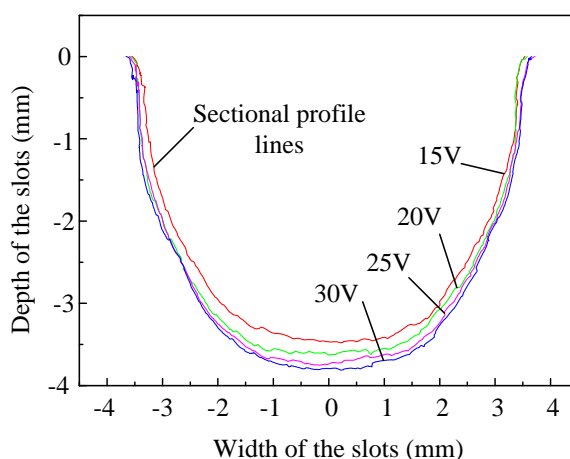


Figure 10. Cross-sectional profiles of machined grooves under different voltages.

### 4.3 Post-machining using electrochemical grinding

According to the results presented thus far, processing is efficient and stable at an applied voltage of 30 V. In this section, the workpiece is first pre-machined with an applied voltage of 30 V and then post-machined to provide good surface quality. During post-machining, tool B first feeds in the vertical direction and then feeds horizontally to the left and right. The finish-machining allowance in the vertical direction is 0.85 mm, while the total finish-machining allowance in the horizontal direction is 1.3 mm. The specific finish machining conditions employed are shown in Table 4.

**Table 4.** Post-machining parameters.

Parameter	Value
Tool type	B
Applied voltage, V	1
Electrolyte pressure, MPa	0.2
Depth of cut, mm	0.025
Feed rate, mm·min <sup>-1</sup>	30
Electrolyte temperature, °C	30

Fig. 11 shows cross-sectional photographs of slots produced by combining pre- and post-machining. After post-machining, the maximum slot depth is 3.85 mm, which is the sum of the pre-machining cut depth (3 mm) and vertical finish-machining allowance (0.85 mm). The excess depth decreases from 27% after pre-machining to 0% after post-machining. This indicates that no stray corrosion occurs during post-machining.

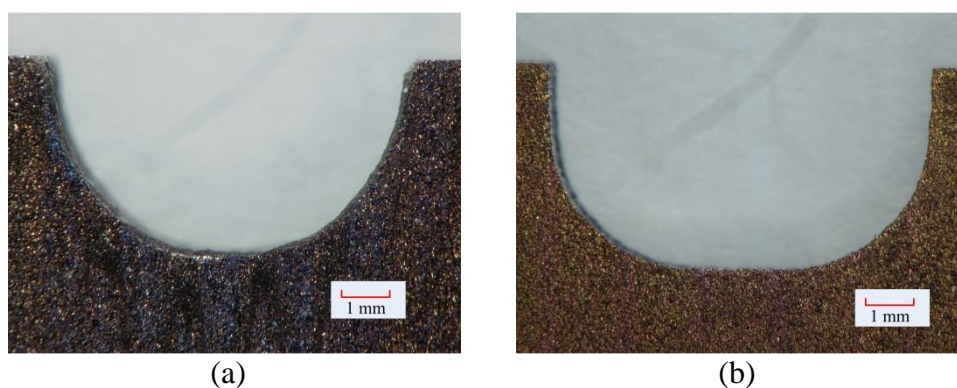


**Figure 11.** Comparison of groove sections at different stages: (a) after pre-machining with tool A and (b) after post-machining with tool B.

Fig. 12 compares the machined surfaces. The surface quality is poor before post-machining. It is uneven and contains a large amount of insoluble residue. However, the surface quality clearly improves after electrochemical grinding, even gaining metallic luster. Quantitatively, the surface roughness can reach Ra 4.853  $\mu\text{m}$  after electrochemical milling but is reduced by approximately 92% to Ra 0.372  $\mu\text{m}$  after electrochemical grinding. The surface roughness is higher than Ra 5  $\mu\text{m}$  when Mishra [24] performs

electrochemical milling in a  $\text{NaNO}_3$  solution. Combined machining can significantly improve the machined surface roughness.

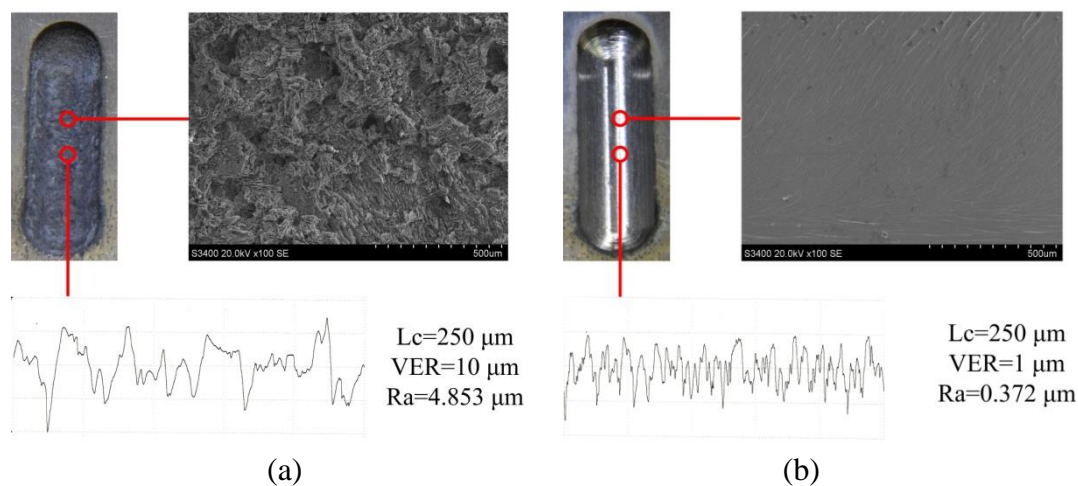


**Figure 12.** Comparison of machined surfaces at different stages: (a) after pre-machining with tool A and (b) after post-machining with tool B.

## 5. CONCLUSIONS

This paper presents a method of machining Ti-6Al-4V alloy using electrochemical milling and grinding and studies its performance. It shows that the combined process can machine Ti-6Al-4V with high efficiency and good surface quality. It has significant application potential in the aircraft manufacturing industry. The conclusions drawn are:

1) The measured Ti-6Al-4V dissolution potential in 10%  $\text{NaNO}_3$  solution was 11 V. When the pre-machining applied voltage increased from 15 V to 30 V, the maximum feed rate increased from  $1.2 \text{ mm} \cdot \text{min}^{-1}$  to  $2.2 \text{ mm} \cdot \text{min}^{-1}$  and the MRR increased from  $22.88 \text{ mm}^3 \cdot \text{min}^{-1}$  to  $40.62 \text{ mm}^3 \cdot \text{min}^{-1}$ . The depth of cut used in this experiment was 3 mm.

2) The maximum machined groove depths noted in the pre-machining stage increased with the applied voltage within the 15 V–30 V range. When the applied voltage increased from 15 V to 30 V, the maximum groove depth increased from 3.48 mm to 3.81 mm, with the excess groove depth increasing from 16% to 27%.

3) After post-machining via electrochemical grinding (the workpiece was first pre-machined using electrochemical milling with an applied voltage of 30 V), the excess groove depth decreased from 27% to 0% and the surface roughness was reduced by about 92% from  $R_a 4.853 \text{ μm}$  to  $R_a 0.372 \text{ μm}$ .

## ACKNOWLEDGMENTS

This work was supported by the National Natural Science Foundation of China (Grant No. 51875286) and the Postgraduate Research & Practice Innovation Program of Jiangsu Province (Grant No. SJCX18\_0107).

## References

1. J. Babu and A. Dutta, *J. Mater. Res. Technol.*, 4 (2015) 348.
2. Y.F. Zhang, J.Z. Li and S.H. Che, *Int. J. Electrochem. Sci.*, 13 (2018) 4792.
3. Y. Liu, S.W. Tang, G.Y. Liu, Y. Sun and J. Hu, *Int. J. Electrochem. Sci.*, 11 (2016) 10561.
4. S.Y. Hong, I. Markus and W.C. Jeong, *Int. J. Mach. Tool. Manu.*, 41 (2001) 2245.
5. M. D. Moses and M. P. Jahan, *Int. J. Adv. Man. Tech.*, 81 (2015) 1345.
6. H. Demirtas, O. Yilmaz and B. Kanber, *J. Mater. Process. Technol.*, 262 (2018) 585.
7. K.P. Rajurkar, D. Zhu, J.A. McGeough, J. Kokaz, and A. De Silva, *CIRP Ann.*, 48 (1999) 567.
8. S. Hinduja and J. Pattavanitch, *CIRP J. Manuf. Sci. Tech.*, 12 (2016) 79.
9. W.D. Liu, S.S. Ao, Y. Li, Z.M. Liu, H. Zhang, S. M. Manladan, Z. Luo and Z.P. Wang, *Electrochim. Acta*, 233 (2017) 190.
10. X.D. Wang, N.S. Qu, P.F. Guo, X.L. Fang and X. Lin, *J. Electrochem. Soc.*, 164 (2017) E548.
11. W. Vanderauwera, M. Vanloffelt, R. Perez and B. Lauwers, *Procedia CIRP*, 6 (2013) 356.
12. G.X. Liu, H.P. Luo, Y.J. Zhang, J. Qian, J.W. Liu and C.H. Liu, *Int. J. Adv. Manuf. Technol.*, 85 (2016) 191.
13. S. Niu, N.S. Qu, S.X. Fu, X.L. Fang and H.S. Li, *Int. J. Adv. Manuf. Technol.*, 93 (2017) 2123.
14. X.L. Fang, N.S. Qu, Y.D. Zhang, Z.Y. Xu and D. Zhu, *J. Mater. Process. Technol.*, 214 (2014) 556.
15. D.Y. Wang, Z.W. Zhu, J. Bao and D. Zhu, *Int. J. Adv. Manuf. Technol.*, 76 (2015) 1365.
16. H.S. Li, S. Niu, Q.L. Zhang, S.X. Fu and N.S. Qu, *Sci. Rep.*, 7 (2017) 3482.
17. A. Hascalik and U. Caydas, *J. Mater. Process. Technol.*, 190 (2007) 173.
18. D.T. Curtis, S.L. Soo, D.K. Aspinwall and C. Sage, *CIRP Ann. Manuf. Technol.*, 58 (2009) 173.
19. Y.Y. Wang and N.S. Qu, *Int. J. Electrochem. Sci.*, 14 (2019) 1116.
20. Y.Y. Xu, J. Wang, X.L. Zhang, P. Wang, J.H. Shi and F. Huo, *Int. J. Electrochem. Sci.*, 12 (2017) 10308.
21. K.W. Mao, *J. Electrochem. Soc.*, 118 (1971) 1876.
22. M. Datta, H.J. Mathieu and D. Landolt, *J. Electrochem. Soc.*, 131 (1984) 2484.
23. D.Y. Wang, Z.W. Zhu, B. He, Y.C. Ge and D. Zhu, *J. Mater. Process. Technol.*, 239 (2017) 251.
24. K. Mishra, D. Dey, B.R. Sarkar and B. Bhattacharyya, *J. Mater. Process.*, 29 (2017) 113.
25. S. Niu, N.S. Qu and H.S. Li, *Int. J. Adv. Manuf. Technol.*, 97 (2018) 1371.
26. H.S. Li, S.X. Fu, S. Niu and N.S. Qu, *Int. J. Electrochem. Sci.*, 13 (2018) 6608.
27. X.D. Wang, N.S. Qu and X.L. Fang, *J. Mater. Process. Technol.*, 264 (2019) 240.